PAPER





Three-dimensional flow characterization in a joint with plumose pattern

Benoit Nigon 1,2 • Andreas Englert 2 • Christophe Pascal 2

Received: 19 January 2018 / Accepted: 5 August 2018 / Published online: 22 August 2018 © Springer-Verlag GmbH Germany, part of Springer Nature 2018

Abstract

This work numerically simulates fracture flow in natural fractures, specifically in a joint with plumose pattern. A natural fracture surface, previously measured in the field using LiDAR scanning, was used to rebuild an open fracture geometry, assuming mode 1 fracture opening. Three-dimensional fracture flow was modeled by solving Stokes equation in a stationary regime using the finite element method. Three different pressure gradients and apertures were numerically investigated to better understand the impact of plumose patterns with different degrees of roughness. Resulting fracture flow fields were characterized by hydraulic aperture and by statistics on the directional components of the three-dimensional velocity vector. The results show that the hydraulic aperture and the longitudinal component of the velocity vector decrease with increasing roughness. Beyond this classical finding, the study shows that the variance of the longitudinal component of the flow velocity vector also decreases with increasing roughness. This behavior can be predicted based on variance estimates connected to the parabolic profile. The results further revealed that the variances of the transverse components of the velocity vector increase with fracture surface roughness. These findings suggest that the roughness-induced reduction in the mean and the variance of the longitudinal component of the velocity vector in joints with rough surfaces is accompanied with a simultaneous increase of the transverse components of the three-dimensional velocity vector.

Keywords Fractured rocks · Natural fractures · Numerical modeling · Fracture flow

Introduction

Fractured geological formations are omnipresent in ground-water systems. To deepen knowledge about the circulation of water, hydrothermal fluids and contaminants, a better understanding of fractured aquifers is of prime importance to many scientific and engineering fields (Berkowitz 2002; Zhao et al. 2008). In applied geoscientific modelling, natural fracture systems are usually simplified by parallel planes. Approaches using measurements of natural fracture surfaces have become less challenging due to recent advances in instrumentation and computational power. Thus, modelling real fracture surfaces might improve fracture models and provide better insight into physical processes associated with rough fractures. Nowadays, developing a more comprehensive understanding

quickly progressing topic in hydrogeology (Zimmerman et al. 1991; Mourzenko et al. 1995; Ge 1997; Oron and Berkowitz 1998; Méheust and Schmittbuhl 2001; Zhao et al. 2004; Neuman 2005; Schmittbuhl et al. 2008; Guha Roy and Singh 2016; Luo et al. 2016; Chen et al. 2016; Chen et al. 2017) and particularly relevant for geothermal processes (Bodvarsson 1972; Gringarten et al. 1975; Bodvarsson and Tsang 1981; Pruess et al. 2005; Grant et al. 2013; Suzuki et al. 2016; Guo et al. 2016), and contaminant transport in fractures (Tang et al. 1981; Nicholl and Detournay 2001; Becker and Shapiro 2003; Zhao et al. 2007; Boschan et al. 2008; Auradou 2009; Fomin et al. 2011; Kang et al. 2015; Zou et al. 2017). Also, extensive studies demonstrated that in naturally formed fractures and cracks, physical and chemical dissolution instability can create cracks and preferential flow channels in fluid-saturated rocks (Zhao et al. 2016, 2017). Only a few studies that numerically investigate flow associated with real fracture geometries have been carried out (Cardenas et al. 2007; Watanabe et al. 2013; Ishibashi et al. 2015; Zou et al. 2017). The integration of measured fracture apertures in these models is often derived from µCT-Scan measurements. Such measurements are, however, usually

of flow and transport in fractured rocks is a challenging but



[☑] Benoit Nigon benigon@hotmail.fr; benoit.nigon@hs-bochum.de

International Geothermal Center, Bochum, Germany

Institute of Geology, Mineralogy and Geophysics, Ruhr University Bochum, Bochum, Germany

severely limited in spatial scale due to sample dimensions that are below the order of tens of centimeters. A gap in spatial resolution exists between the laboratory scale and the field scale, and meso-scale studies for joint systems, representing the most frequent type of fractures in rocks, are rare (Pollard and Aydin 1988). Furthermore, joint surfaces often display plumose patterns with its associated features like hackles and rib marks. To the authors' knowledge, the impact of these characteristic features on fracture flow has never been investigated thoroughly.

In rough fractures, flux variability is mainly controlled by fracture roughness and aperture variability (Witherspoon et al. 1980). The commonly used parallel plate model assumes that fracture transmissivity is proportional to the cube of mechanical aperture (Witherspoon et al. 1980). However, it has been shown that the fracture transmissivity of a rough wall deviates from its parallel plate equivalent (Zimmerman et al. 1991; Mourzenko et al. 1995; Ge 1997; Oron and Berkowitz 1998; Luo et al. 2016; Chen et al. 2017), a deviation that was described as a consequence of preferential flow pathways (i.e. flow channelling) associated with the rough fracture (Brown 1987; Zimmerman et al. 1991; Park and Hahn 1998; Le Goc et al. 2010; Vilarrasa et al. 2011; Lavrov 2013; Chen et al. 2017). Flow channelling is controlled by fracture surface fluctuation and the contact areas existing between fracture walls (Dijk and Berkowitz 1999; Méheust and Schmittbuhl 2001; Auradou et al. 2005; Watanabe et al. 2008; Zou et al. 2017). Many fracture transmissivity estimations in modelling were obtained using the Reynolds equation with lubrication theory (Zimmerman et al. 1991; Nicholl et al. 1995; Neuville et al. 2011). Taking the Stokes equation as a reference, Mourzenko et al. (1995) have shown that using Reynolds' equation leads to an overestimation of flow velocity if the fracture aperture is small and aperture fluctuations are high. The Stokes equation is a simplification of the Navier-Stokes equation in which the inertial term is removed. The Navier-Stokes equation was used to compute fracture flow at high Reynolds numbers (Brush and Thomson 2003; Zimmerman et al. 2004; Boutt et al. 2006; Crandall et al. 2010; Bouquain et al. 2011; Zou et al. 2017). The deviation between Stokes and Navier-Stokes occurs when velocity (i.e. pressure gradient and mean aperture) and aperture fluctuations increase. The Navier-Stokes equation is favoured for the simulation of eddies which reduce mean flow velocity and consequently decrease hydraulic aperture. However, this process was shown to occur for Reynolds numbers higher than 10 (Zimmerman et al. 2004; Auradou 2009; Briggs et al. 2017). In hydrogeological conditions for low flow velocities, low Reynolds numbers (Re < 1) and smooth variations of fracture apertures (in particular in the case of matching surfaces), it appears reasonable to favour Stokes equation (Méheust and Schmittbuhl 2001; Brush and Thomson 2003; de Dreuzy et al. 2012; Chen et al. 2017; Lee et al. 2014).

Furthermore, Zimmerman et al. (2004) have shown that a weak inertial term regime exists between Re = 1 and Re = 10.

Empirical relationships between hydraulic and mechanical aperture exist. The major difference between hydraulic and mechanical aperture arises from fracture surface roughness. Fracture surfaces are often characterized by means of using roughness parameters such as the joint roughness coefficient, Z2 roughness parameter, correlation length or Hurst exponent. Subsequently, studies were carried out to link fracture flow to roughness parameters (Talon et al. 2010; Li and Jiang 2013) for example, Li and Jiang (2013) and Zhao et al. (2014) modeled fracture flow for different fracture configurations and with various fracture surfaces, as characterized by different Z2 roughness parameter (i.e. Z2 ranging from 0 to 0.5) in the cases of one single fracture and a fracture network respectively. They showed that the difference between mechanical and hydraulic aperture increases with roughness. Because of strong variability of roughness directional anisotropy as a function of location on the surface, for the specific case of a joint, depicting a plumose pattern, a unified estimation of roughness parameters for the entire fracture surface is not appropriate (Nigon et al. 2017). Consequently, the direct link between common roughness parameters and hydraulic aperture cannot be made and a derived method must be applied.

The present study aims to model and characterize mesoscale fracture flow (approx. 62 cm × 62 cm). To improve the understanding of fracture flow in joints, high-resolution LiDAR scans of a joint surface were used which were previously acquired (Nigon et al. 2017). The selected joint surface exhibits S-type plumose patterns. Assuming mode 1 fracture opening, a three-dimensional (3D) fracture was rebuilt by duplicating the measured surface. The fracture flow in the stationary regime was solved with Stokes equations. A series of model configurations involving various pressure gradients, apertures and roughness amplitudes were computed and compared to parallel plate models. Fracture flow was characterized by hydraulic aperture, probability distribution functions (pdf) and cumulative distribution functions (cdf) of directional velocity field components. Furthermore, the sensitivity of the flow results was analyzed with regard to surface roughness, aperture and pressure gradient.

Materials and methods

Fracture surface measurements and aperture rebuilding

To investigate the impact of plumose patterns on fracture flow, a previously scanned joint fracture surface was used (Nigon et al. 2017). A freshly excavated fracture developed in Turonian glauconitic sandstones of the Klieve quarry, Münsterland, Western Germany, was selected for this study. The joint



surface morphology exhibits the S-type plumose structure characterized by quasi-symmetrical structures and a straight propagation axis. Fracture surface measurements were performed by the use of light detection and ranging (LiDAR) technology. Details on the acquisition and the processing of the data are given in Nigon et al. (2017). The joint surface characterization revealed a strong anisotropic impact of plumose patterns on the Hurst exponent and correlation length. The Hurst exponent varies from 0.4 to 0.8 through all scales of investigation and is, as well as the correlation length, dependent on the location on the surface (Nigon et al. 2017). Surface elevation varies from -2.7 to 3.7 mm with a standard deviation of 1.2 mm. In the following, the more common term of roughness is used instead of plumose pattern (a plumose pattern being the characteristic morphology that roughness often takes on a joint surface).

To rebuild the joint at a mesoscopic scale, the S-type joint surface was treated as an expected mode 1 fracture. Accordingly, the measured surface in Fig. 1 is assumed to be symmetric and matching the second fracture wall. The measured joint surface (surface elevations in Fig. 1) was duplicated and stacked; thus, the generated joint consists of two perfectly matching surfaces. The distance separating both surfaces corresponds to the mechanical aperture. In this study, three mechanical apertures of 1, 3, and 5 mm were investigated.

Models consider a plane wall configuration, a natural roughness configuration (as described before) and a twofold natural roughness configuration. The twofold natural roughness configuration is derived by multiplying the natural roughness configuration by two. Taking into consideration the plumose patterns and the maximum relief resulting from these configurations, the modeled geometry is very similar to

what would be expected naturally. Instead of using other measured surfaces using LiDAR, these modifications allowed us to better understand and characterize flow in joints without drastically changing the geometry of the fracture.

Basics of fracture flow

Fracture flow was computed using Stokes equation representing a simplification of the Navier-Stokes equations. For Navier-Stokes with low Reynolds numbers the diffusive term overrides the convective term, consequently the inertial term can be removed according to (Mourzenko et al. 1995)

$$-\nabla P + \mu \nabla^2 u = 0 \tag{1}$$

with pressure P, viscosity μ , and fluid velocity u.

Fracture flow simulation with Stokes equation is applicable to small fracture apertures, low flow velocities, and smooth variations of fracture aperture (i.e. matching surfaces have smoother variation of aperture than the roughness itself). In the case of parallel and smooth planes, only the component in the main flow direction is nonzero and the equation can be simplified. Using Poiseuille's plane configuration, flow through a fracture is determined by the cubic law (Zimmerman et al. 1991)

$$Q = \frac{-a^3(\mathbf{x}, \mathbf{y})}{12\mu} \nabla P \tag{2}$$

where Q is flow in $[m^3/s]$ and a aperture in [m].

In this study, flow characterization focuses on the X, Y and Z components of the velocity vector and their respective statistics. To validate the quality of the model for plane wall configurations and to compare the results between plane and

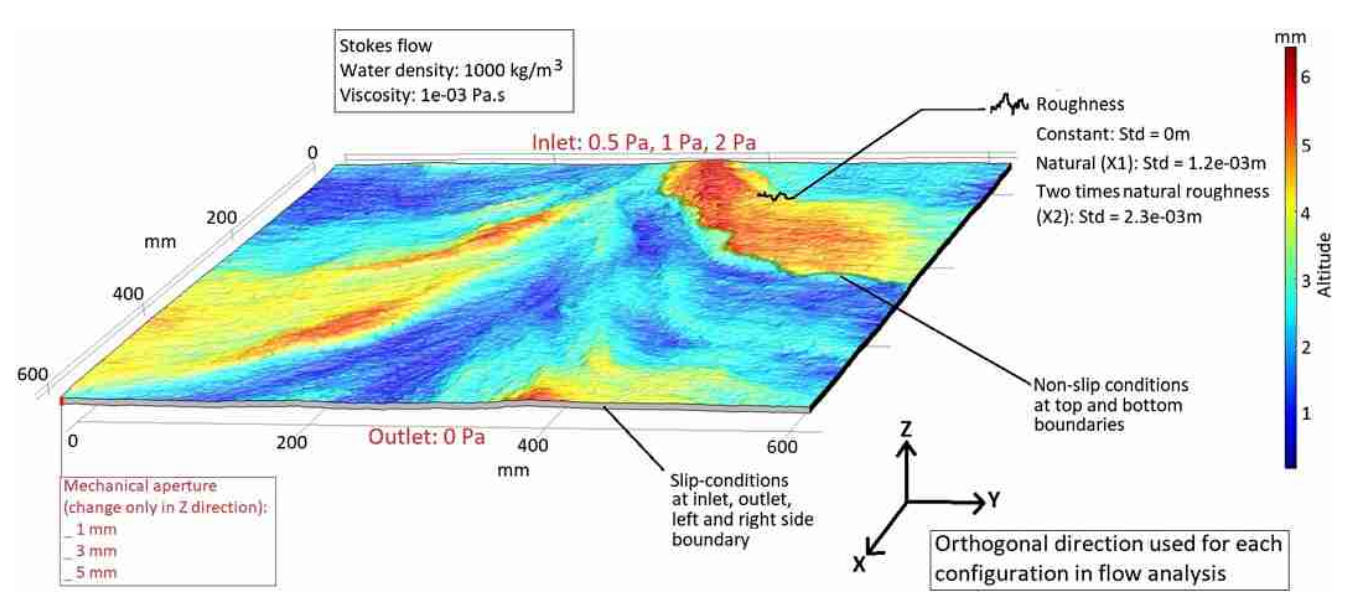


Fig. 1 Summary of the flow modeling set up; fracture natural roughness was derived from LiDAR scan measurements [Natural (X1)]



rough fractures, the parabolic velocity profile in the fracture is calculated according to (Coursenotes 2009)

$$v_{x} = \frac{H^{2}}{2\mu} \left[\frac{\partial P}{\partial x} \left(\frac{z^{2}}{H^{2}} - 1 \right) \right]$$
 (3)

where *H* is half aperture, $\frac{\partial P}{\partial x}$ pressure gradient and *z* position. The maximum velocity of the parabolic profile is computed by (Coursenotes 2009)

$$U_{\text{max}} = -\frac{\partial P}{\partial x} \frac{a^2}{2\mu} \tag{4}$$

By using the relationship between average velocity of the parabolic profile and maximum velocity, equivalent average velocity in the fracture is (Coursenotes 2009)

$$U_{\text{avg}} = \frac{2}{3} U_{\text{max}} \tag{5}$$

One can rewrite Eq. (3) to calculate hydraulic aperture by inserting mean flow velocity from the models according to

$$a_{\rm h} = \sqrt{\frac{24U_{\rm avg}\mu L}{2P}} \tag{6}$$

where a_h is hydraulic aperture, L fracture length in the main flow direction, and P pressure difference.

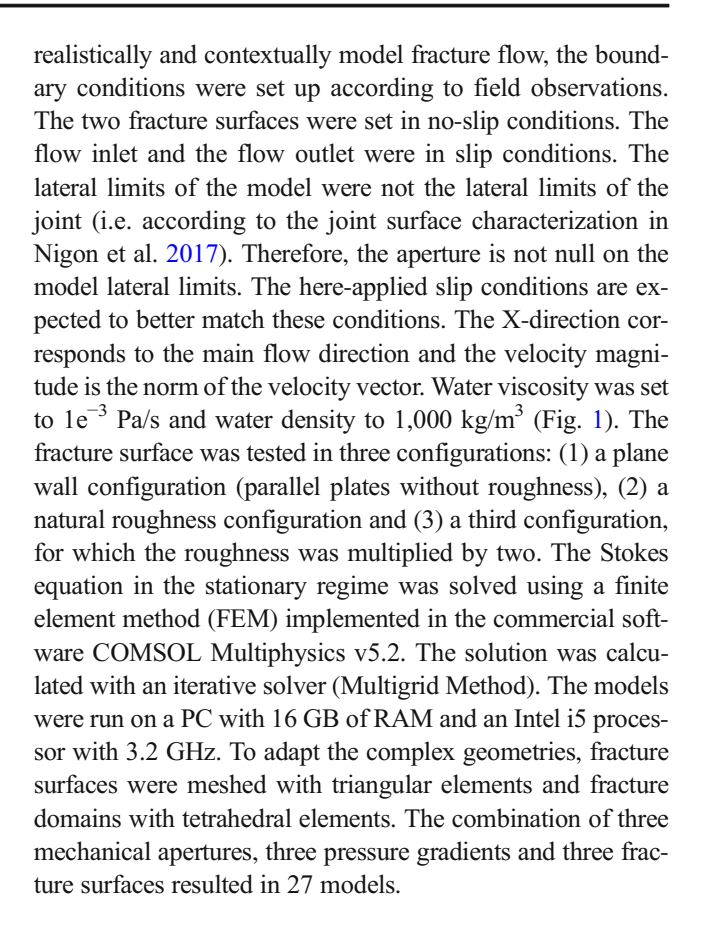
The fracture flow characterization is, in parts, based on the analysis of variance of directional components of velocity vectors. The variance of the X components of the modelled velocity vector was compared to the variance of their counterparts for an equivalent plane wall configuration. The term "theoretical variance" in the paper corresponds to the calculated variance of the parabolic velocity profile resulting from Eq. (3) by varying pressure gradient and fracture aperture. The variance of the results of the modeling corresponds to the calculated variance of the probability density function (pdf) for the chosen directional velocity component.

Numerical flow modeling

Set up of the models

Fracture flow was calculated using the Stokes equation in the stationary regime. The size of the model in X and Y directions is 625.5 mm. For model dimensions according to Z, three configurations were modeled with respective distances of 1, 3 and 5 mm.

Fracture flow was computed with 1, 3, and 5-mm mechanical aperture, respectively. Three pressures, 0.5, 1 and 2 Pa, were imposed at the fracture inlet. At the outlet of the fracture, pressure was set to 0 Pa. Throughout the paper pressure at the inlet was used as reference (0.5, 1 and 2 Pa). Pressure gradients correspond to 0.8, 1.6 and 3.2 Pa/m, respectively. To



Mesh convergence and numerical errors

Each individual model was validated. For the plane wall configurations, the local parabolic velocity profile was derived from the analytical solution (Eq. 3) and compared with the results of the modeling (Fig. 2d). For the rough fracture configurations, mesh convergence studies were performed on mean fracture flow velocities and variances of the X, Y and Z components of the velocity vectors (Fig. 2a-c). The mesh convergence was performed by first increasing the density of triangular elements on the fracture surface and then increasing the density of tetrahedral elements in the fracture domain. This process was repeated until the selected values (i.e. mean flow velocity and variance of the directional component of the velocity vector) remained stable. The configuration, 5 mm twotimes natural roughness, shown in Fig. 2, is composed of 4,486,814 tetrahedral elements and 758,138 triangular elements. In comparison, the configuration 1-mm one-time natural roughness is composed of 2,211,120 tetrahedral elements and 1,392,246 triangular elements.

As visualized in Fig. 2a, for the configuration 5 mm and two times natural roughness with 1 Pa inlet pressure, the mean flow velocity magnitude and that in the X direction converge already with 1.0×10^6 elements. The variance of the X components of the velocity vectors converges with $\sim 4.0 \times 10^6$ elements. A similar behavior can be observed in the Y and Z



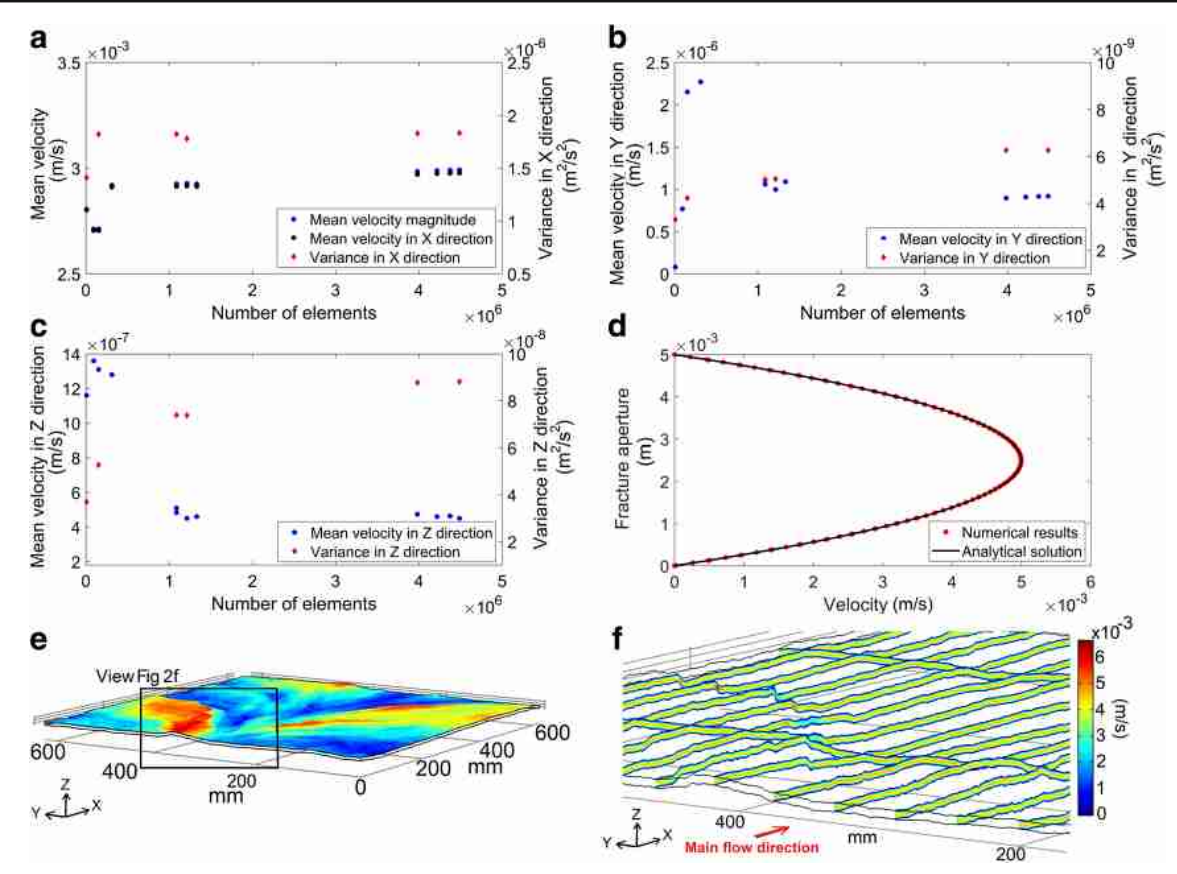


Fig. 2 Examples of model validation. **a** Mesh convergence analysis on flow velocity magnitude, flow velocity and variance of flow velocity in the X direction for the configuration: 5 mm and two times natural roughness with 1 Pa inlet pressure. **b** Mesh convergence analysis on flow velocity and variance of flow velocity in Y direction for configuration: 5 mm and two times natural roughness with 1 Pa inlet pressure. **c** Mesh convergence analysis on flow velocity and variance of

flow velocity in Z direction for configuration: 5 mm and two times natural roughness with 1 Pa inlet pressure. d Comparison of analytic solution with velocity in X direction for configuration: 5 mm and two times natural roughness with 1 Pa inlet pressure. e 3D view of the joint indicating the location of the (f). f Cross-sections of velocity magnitude in X–Z and Y–Z directions in the fracture, according to the location (e)

directions (Fig. 2b,c). Once the models converged, a directional flow heterogeneity according to X, Y and Z components of the velocity vectors is evidenced (Fig. 2f). According to the location in the fracture domain (Fig. 2e), flow heterogeneities vary as a function of their respective positions along the plumose. The plane wall configuration numerical results are almost identical to the analytical solution for the 5 mm plane wall configuration with 1 Pa pressure inlet (Fig. 2d).

A small amount of negative velocity values is modeled for configurations with two times natural roughness (i.e. the most numerically demanding case). The amount of negative values was quantified and shown to contribute only a small percentage to the velocity distribution in the fracture. Moreover, inspecting all configurations, a maximum of $5.52 \times 10^{-5}\%$ of negative values was found. Therefore, the modeled negative velocities values were considered as negligible in the calculation of both hydraulic aperture and variance.

An estimation of the numerical errors was derived from the mesh convergence studies. Taking the example of the configuration 5 mm and two times natural roughness (i.e. combination for highest velocity and highest flow heterogeneities, Fig. 2), the standard deviation for variance/mean flow velocities based was calculated on the 3.98×10^6 elements and 4.48×10^6 elements cases (Fig. 2a–c). For the mean flow velocity in X, Y, and Z directions, the standard deviations amount to 2.78×10^{-6} , 1.04×10^{-8} and 9.86×10^{-9} m/s, respectively. For the variance of the X, Y and Z components of velocity vectors, the standard deviations are 7.00×10^{-9} , 1.62×10^{-12} and 3.35×10^{-10} m²/s², respectively. These results suggest that the numerical error is at least two orders of magnitude smaller than velocity statistical estimates.

Results

Pressure field

A pressure field resulting from solving the Stokes equation for the configuration 5 mm and two times natural roughness is shown in Fig. 3. Pressure fields for other models with



rough fracture surfaces exhibit similar patterns. For the plane wall configuration, strictly parallel isobars are arranged perpendicular to the main flow (X-) direction. In general, quasiparallel isobars are modelled and do not show major variability for the full fracture domain shown (Fig. 3). However, by focusing on the main hackles of the plumose structure (e.g. a well-marked hackle can be seen at the top left of Fig. 3 and at the top right of Fig. 1) pressure field disturbances are observed according to Y. At the corresponding locations, the isobars are also disturbed according to Z. For rough fractures with natural roughness, similar perturbations of the modelled isobars are found but are less pronounced. At smaller spatial scale (i.e. several centimetres) small variations of the isobars are modeled and are due to joint plumose patterns of relatively smaller scale.

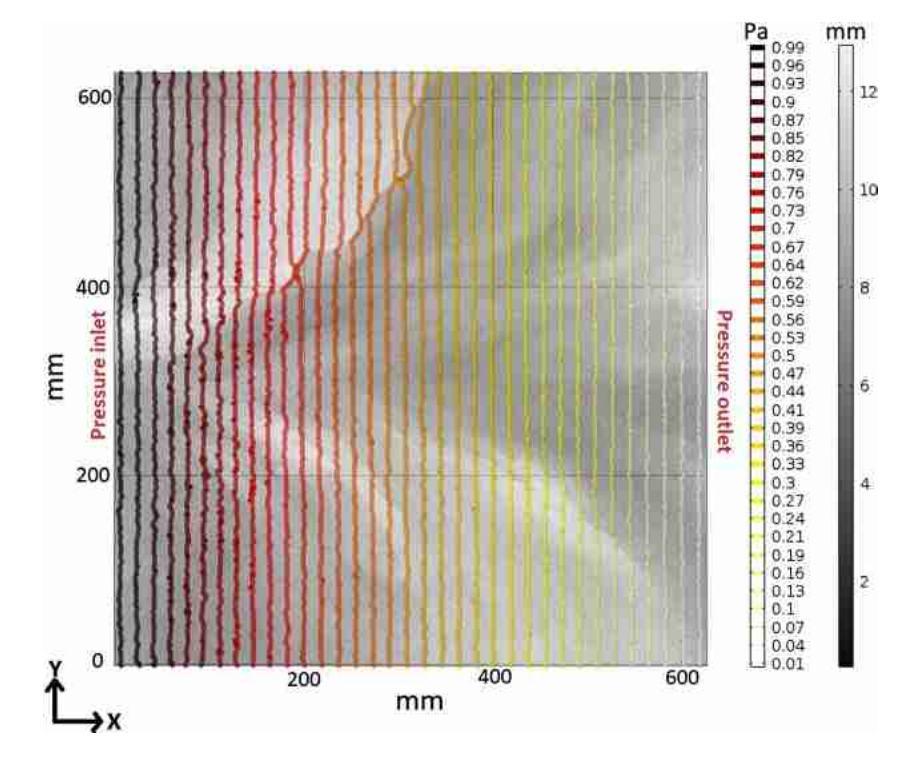
Flow field in a rough joint

To date, a formal and unified description of local hydraulic apertures in fractures does not exist (Mourzenko et al. 1995; Ge 1997; Oron and Berkowitz 1998). Considering the uncertainties found in local hydraulic aperture definitions, the flow within joints was characterized using flow velocity magnitude and the X, Y and Z components of the velocity vectors. This allowed us to separate and individually analyze every velocity term in a clear and robust way. In this section, a detailed investigation of the flow velocity components for the configuration 3 mm and two times natural roughness is performed. Thereafter, the directional

components of the velocity vectors of a rough fracture configuration are compared to their counterparts, as derived from the modeling of parallel plates with equivalent mechanical aperture (Fig. 4).

The pdf and cdf of velocity magnitudes for the rough fracture and plane wall fracture are both skewed distributions. The plane-wall-fracture configuration reflects the expected pdf for a parabolic velocity profile. The highest frequency corresponds to the maximum velocity (and to predictions of Eq. 4). Velocities decrease with their respective frequencies towards zero. For the pdf and cdf of the rough fracture (Fig. 4a) the frequency of the maximum velocity does not correspond to the maximum frequency. For velocities ranging between 0.75×10^{-3} and 1.5×10^{-3} m/s, the rough fracture configuration does not exhibit a "regular" decrease in velocity with frequency as seen for the plane wall fracture. In this range, cdf and pdf of rough fracture surfaces show an irregular decrease in velocity frequency in comparison to the plane-wall-fracture configuration. The rough fracture geometry is associated with a higher probability of local velocities in the range 0.75×10^{-3} and 1.5×10^{-3} 10⁻³ m/s. The pdf and cdf of the velocity vector X components behave similarly as velocity magnitudes. In Fig. 3b, a small number of negative values are depicted for the X component. These values correspond to modeling errors as discussed before. The pdf and cdf of velocity vector Y and Z components are symmetric and centered at 0 m/s (Fig. 4c,d). By comparing Y and Z velocity components to their planewall-fracture counterparts (Fig. 4g,h) and by preserving the

Fig. 3 Pressure field for the configuration 1 Pa inlet, 5 mm aperture and two times natural roughness (view from the top of the fracture). Joint surface elevations are indicated in grey





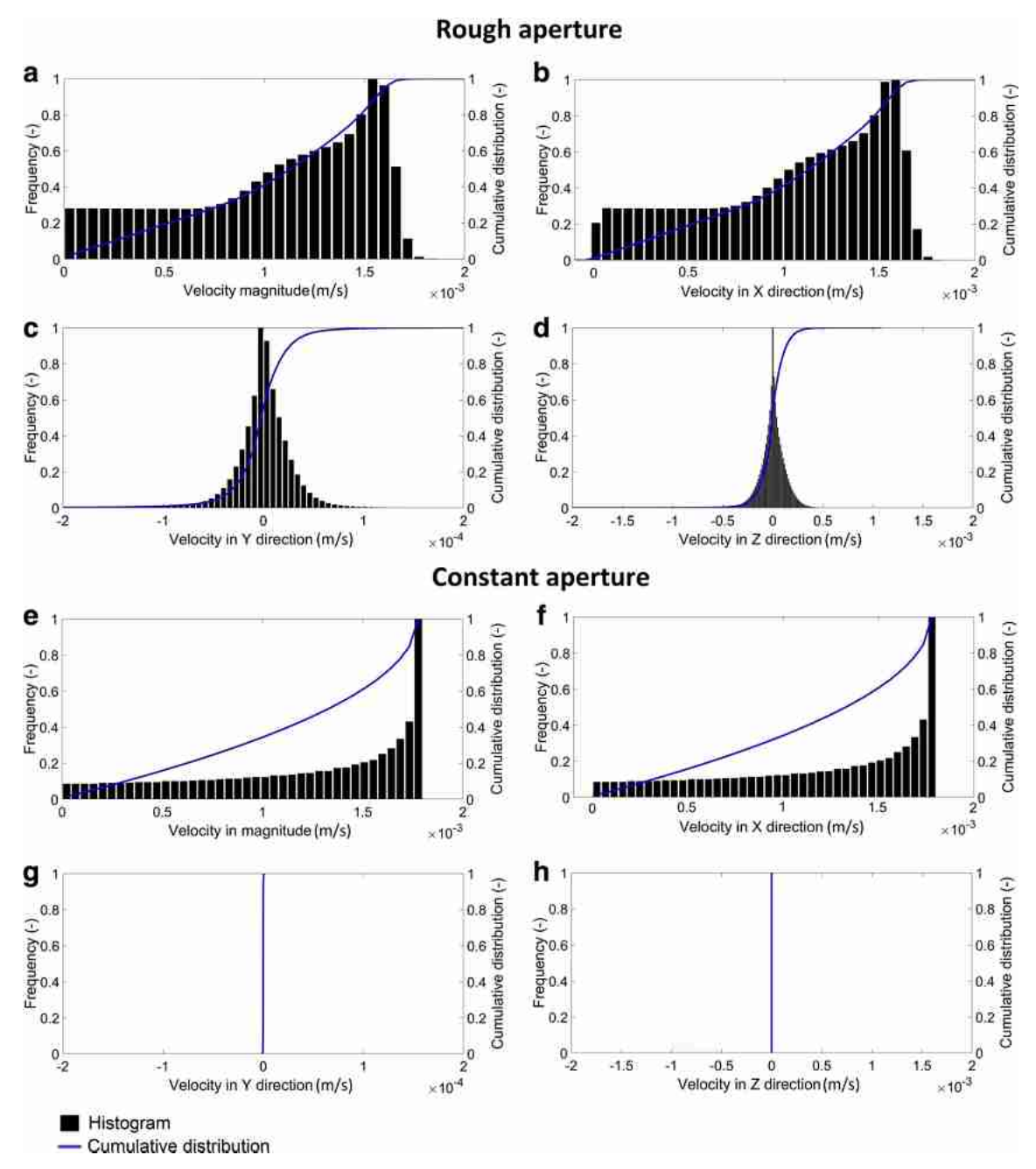


Fig. 4 The probability density function (pdf) and cumulative distribution function (cdf) of velocity components for configuration 3 mm, 1 Pa inlet pressure. **a** pdf and cdf of velocity magnitude, two times natural roughness. **b** pdf and cdf of velocity vector X component, two times natural roughness. **c** pdf and cdf of velocity vector Y component, two times

natural fracture. d pdf and cdf of velocity vector Z component, two times natural roughness. e pdf and cdf of velocity magnitude, plane wall fracture. f pdf and cdf of velocity vector X component, plane wall fracture. g pdf and cdf of velocity vector Y component, plane wall fracture. g pdf and cdf of velocity vector Y component, plane wall fracture.

velocity scale in the abscissa, the plane-wall-fracture configuration appears to be peaks. In Y and Z directions, theoretical results should equal zero; however, modeling does not exactly show zero values, but a variance of the Y and Z components of the velocity vector of 1.87×10^{-14} and $7.45\times 10^{-16}~\text{m}^2/\text{s}^2$, respectively. The discrepancy between theoretical and numerical results are again due to numerical errors, which can only be minimized.

Flow field as a function of aperture and roughness

Cumulative distribution function of velocities and basic statistics thereof

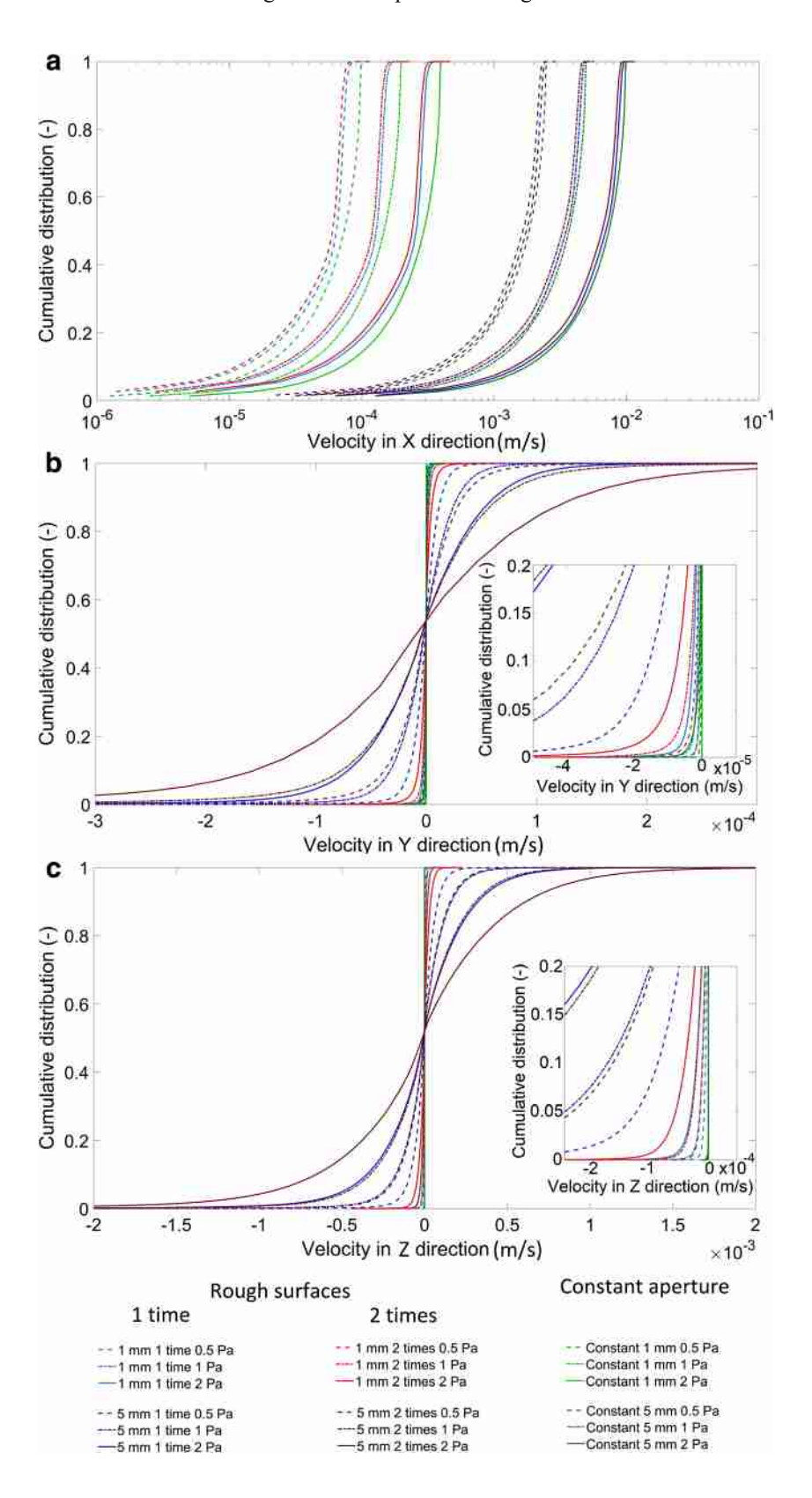
In the following, the cumulative distributions plotted together are studied. It shows how cdf of directional velocity components depends on roughness, aperture and pressure gradient.



In Fig. 5 the impact of roughness, aperture and pressure gradient on the distribution of directional components of the velocity vector is shown.

The shape of the cdf of the velocity X component, for plane-wall-fracture configurations, is insensitive to pressure gradient or aperture changes. It is a characteristic

Fig. 5 Cumulative distribution functions of velocity vector X, Y and Z components. For the sake of clarity, only the 1-smm and the 5-mm configurations are shown. Cumulative distribution of the a X component (main flow direction), b Y component, and c Z component





parabolic velocity profile between parallel plates. When a rough fracture surface is used in fracture flow simulations, a decrease of the mean flow velocity in the X direction is modelled. The decrease in mean flow velocity is accentuated when roughness is increased. With respect to the plane-wall-fracture case, the cdf associated with the rough fracture departs more for the 1-mm aperture than for the 5-mm aperture (Fig. 5a), the 3-mm aperture (not shown here) shows an intermediate behavior. Frequencies corresponding to maximum velocities are significantly lower in rough fractures than in the plane-wall-fracture case. In the normalized frequencies 0.6–0.9, the probability to have velocities close to the mean flow velocity increases due to the geometrical heterogeneities of the rough fracture.

In terms of cdf in Y and Z directions, the use of the rough surface configurations shows significant deviations from the plane wall configuration (Fig. 5b,c). As a consequence of the selected reference frame, mean flow velocities in the Y and Z directions tend to 0 m/s (Fig. 5b,c). The spread of the cdf increases when adding roughness, a phenomenon that is particularly enhanced when pressure gradient and aperture are increased.

The results show a general behavior in accordance with the cubic law. By increasing pressure, the mean flow velocity in the X direction increases linearly. For an aperture change, the mean flow is controlled by the cube of the aperture; however, as the joint walls exhibit more and more roughness, Y and Z components of the flow velocity vector develop and, in turn, reduce mean and variance of the X component of the velocity vector. Figure 6 provides a summary of the mean, median and standard deviation characterizing the flow in X direction for all configurations studied here. It highlights the dependency of the deviation between mean and median velocity and how standard deviation is controlled by fracture surface roughness, aperture and pressure gradient.

Fig. 6 Summary of mean flow velocity, median flow velocity and standard deviation for different configurations shown as a function of surface roughness, pressure and aperture

Hydraulic aperture

The hydraulic aperture was calculated according to Eq. (6) for the 27 investigated models. Figure 7 shows the loss in hydraulic aperture with respect to the mechanical aperture. Results of plane-wall-fracture models show similar hydraulic and mechanical apertures. Their loss in hydraulic aperture is 0%. When heterogeneities (i.e. rough fracture surfaces) are integrated in the models, hydraulic aperture decreases. For all cases, the loss in hydraulic aperture increases when roughness is increased. Furthermore, hydraulic aperture is more affected when mechanical aperture is small. In general, the loss in hydraulic aperture is smaller for a 5-mm mechanical aperture and higher for a 1-mm mechanical aperture.

The impact of pressure gradient on the loss in hydraulic aperture is strongly dependent on mechanical aperture. In cases of small mechanical aperture (i.e. 1 mm), the impact of pressure gradient appears to be negligible (Fig. 7). When mechanical aperture is increased, the loss in hydraulic aperture increases with increasing pressure gradient.

Several authors have shown that flow for variable fracture apertures deviates from the cubic law (Zimmerman et al. 1991; Mourzenko et al. 1995; Ge 1997; Oron and Berkowitz 1998; Luo et al. 2016; Chen et al. 2017). A deviation from the cubic law is often expressed using a ratio between hydraulic aperture and mechanical aperture as a function of normalized mechanical aperture (Renshaw 1995; Méheust and Schmittbuhl 2001, 2003; Al-Yaarubi et al. 2005). The normalization procedure of the mechanical aperture differs amongst the researchers (e.g. mechanical aperture divided by the root mean square (RMS) of roughness, mechanical aperture divided by standard deviation of the aperture, standard deviation divided by mechanical aperture). However, previous studies showed that the ratio hydraulic aperture/mechanical aperture, as a function of normalized mechanical aperture, is generally less than 1 and converges to a sill. Renshaw (1995) estimated

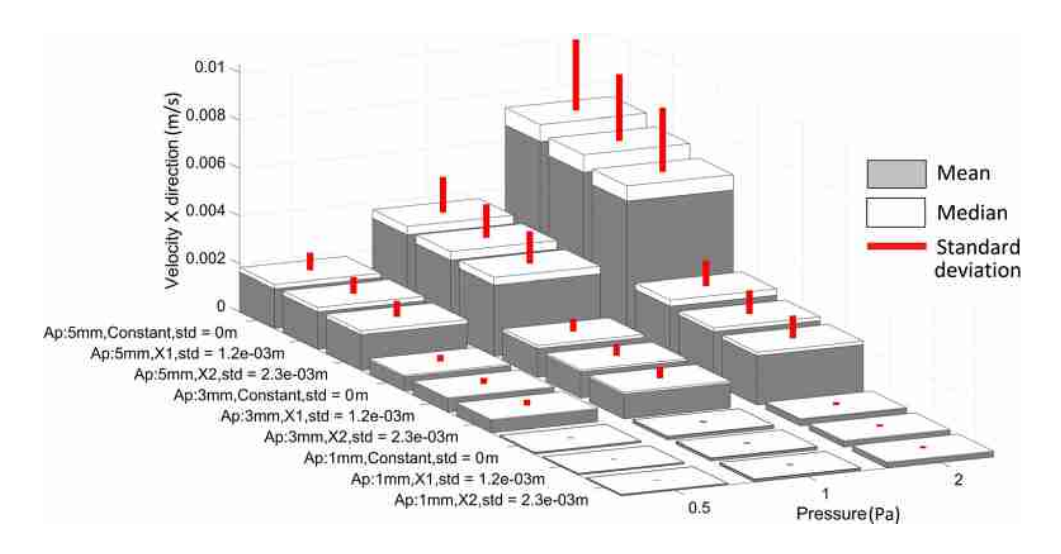
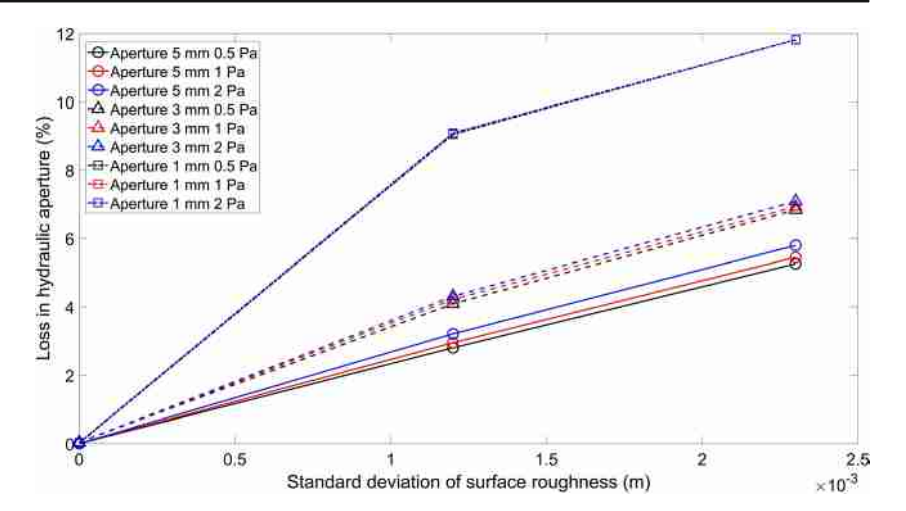




Fig. 7 Percentage of loss in hydraulic aperture as a function of standard deviation of the fracture surface topography



that for low values of the roughness parameter (i.e. arithmetic mean of aperture divided by standard deviation of the aperture <1), the mechanical aperture is higher than the hydraulic aperture. The results show similar trends. In Fig. 7, increase in roughness results in decrease of hydraulic aperture; however, when mechanical aperture increases, the loss in hydraulic aperture is reduced. These trends correspond to convergence to 1 of the ratio of hydraulic aperture on mechanical aperture, as a function of normalized fracture aperture.

Variance of velocity components

The theoretical variance of the velocity X component was calculated directly from the velocity profile resulting from Eq. (3) and increases with pressure gradient and hydraulic aperture. In Fig. 8 the variances for the X components of the velocity vectors are plotted as a function of their respective calculated hydraulic apertures and roughness. The results derived from the plane-wall-fracture models (i.e. denoted "constant" in Fig. 8), plotted as function of their hydraulic apertures, fit their respective theoretical values. Interestingly,

This suggests that even though rough joint surfaces induce a discrepancy between mechanical and hydraulic aperture, the relationship between variance and hydraulic aperture, based on the classic parabolic flow profile, still holds.

For the V components of the velocity vector (Fig. 9a), var-

rough fracture variances also fit the theoretical prediction.

For the Y components of the velocity vector (Fig. 9a), variance increases with increasing aperture, pressure gradient and roughness. Model results for the plane-wall-fracture configuration (SD = 0 m, Fig. 9a) should theoretically be zero, but numerical uncertainties cause nonzero results, which are, however, at least three orders of magnitude lower than their rough fracture equivalents.

For different pressure gradients and aperture configurations, the slope of the transition from natural roughness to twofold natural roughness is similar. This suggests that each pressure gradient aperture configuration exhibits its individual relationship between velocity Y component variance and joint surface roughness; however, all these individual relationships share the same trends.

Velocity Z component variances (Fig. 9b) behave similar to the ones of the Y component. Variances increase with

Fig. 8 Modeled and theoretical variance of flow velocity X component (main flow direction) as function of hydraulic aperture

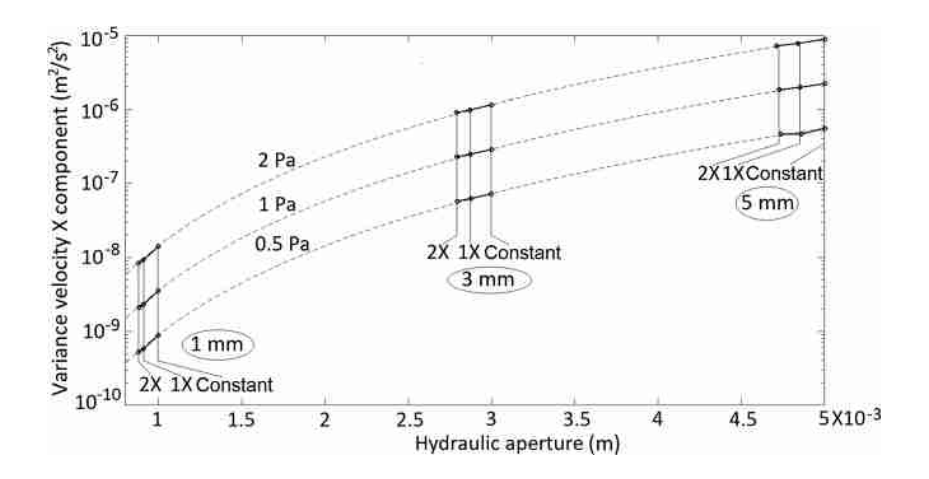
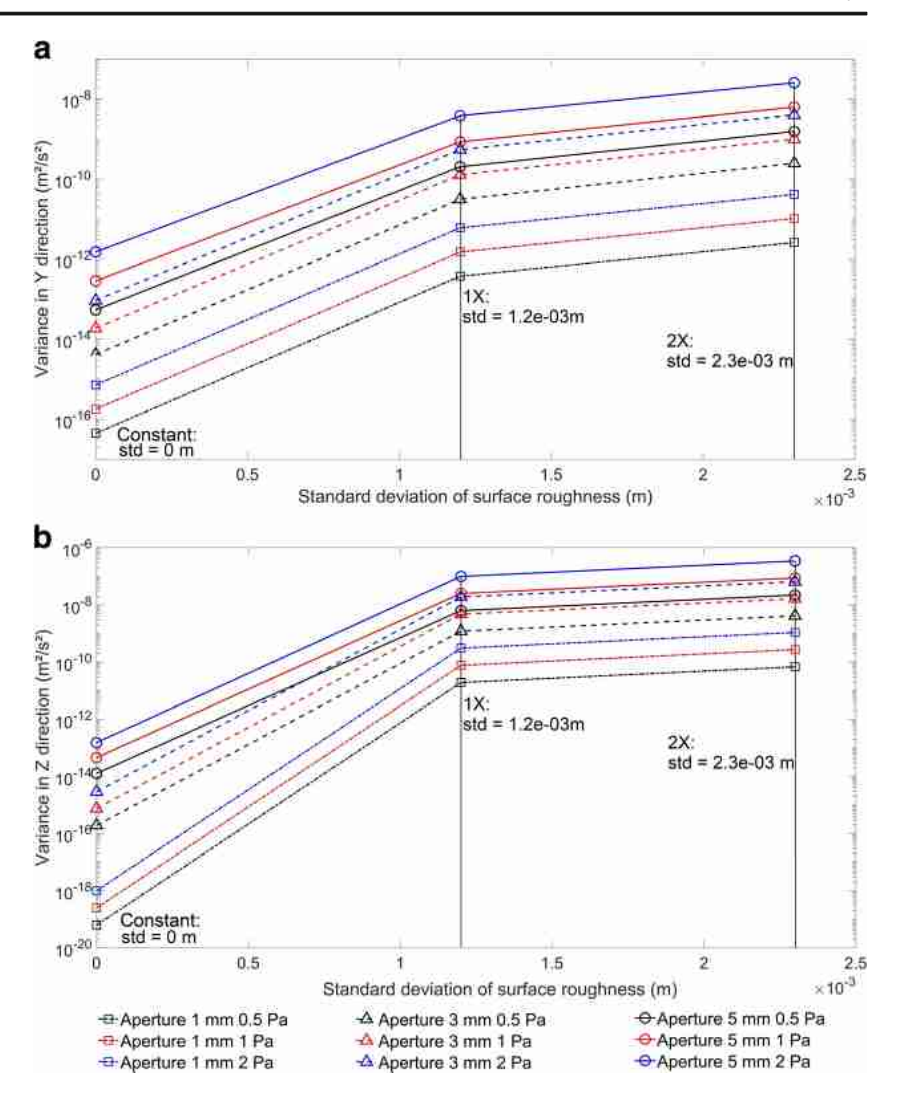




Fig. 9 Variances of the transversal components of the velocity vector as function of roughness: **a** Y component, **b** Z component



increasing apertures, pressure gradients and roughness. The slope of the transition between natural roughness to twofold natural roughness is similar for the different pressure gradients and aperture configurations.

Conclusion

Numerical modeling of flow in a joint with plumose pattern resulted in pressure gradient fields that consist of nearly parallel pressure isolines with small variations caused by the roughness of the joint surface. Only at hackles of the plumose structure, pressure isolines deviate from the overall parallel pattern, indicating stronger variabilities in the pressure gradient fields.

As found in many other studies on rough fracture flow, the numerical modeling results based on a joint with plumose pattern show a decrease of the hydraulic aperture and the mean velocity in longitudinal direction with increasing joint surface roughness. This phenomenon is more pronounced at smaller mechanical apertures and higher-pressure gradients. Within the configurations of this study, a maximum decrease of the hydraulic aperture of 12% was found.

Aside from this well-known phenomenon, the 3D modeling examples allow some deeper insights into the variances of the velocity vector components which accompany the hydraulic aperture decrease as function of joint surface roughness. Thus, the variance of the longitudinal direction of the velocity vector decreases with increasing roughness. Furthermore, the results suggest that the variance of the longitudinal component of the velocity vector can be predicted based on the classical parabolic profile for parallel plates, once the hydraulic aperture is known, for example from field experiments. This finding holds true at least for all the configurations that were numerically modeled in the present study.

From theory, it is well known that the transverse components of the velocity are zero for the cases of parallel plates resulting in a zero variance for the transverse components of the velocity vector. The results show that this is different for flow in joints with rough surfaces. Here the variances of the



velocity vector in transverse directions increase with increasing joint surface roughness. This behavior is different for each mechanical aperture and each pressure gradient; however, the relative increase in the variance of the transverse components of the velocity vector is almost identical for all configurations within the present study.

The results of the present numerical study have shown in detail how far the joint plumose pattern influences flow characteristics in joints with two matching surfaces. In addition to these new insights in fracture flow, these findings could be helpful to the design and positioning of geothermal facilities.

Acknowledgements We acknowledge two anonymous reviewers for their constructive comments. The authors are thankful to Mandy Duda (International Geothermal Centre, Bochum) for her priceless help to improve the quality of the manuscript. We are grateful to Aline Saintot (Ruhr-Universität Bochum) for her help in identifying and performing surface elevation measurements on joints. Also we thank Rolf Bracke (GZB) for his support.

Funding information The first author benefited from a PhD grant from the Applied Research on Enhanced Geothermal Energy System (AGES) graduate school, a joint venture between the International Geothermal Centre Bochum (GZB) and the Institute of Geology, Mineralogy and Geophysics, Ruhr-Universität Bochum.

References

- Al-Yaarubi AH, Pain CC, Grattoni CA, Zimmerman RW (2005) Navier-Stokes simulations of fluid flow through a rock fracture. AGU, Washington, DC, 10 pp
- Auradou H (2009) Influence of wall roughness on the geometrical, mechanical and transport properties of single fractures. J Phys D Appl Phys 42(21):214015. https://doi.org/10.1088/0022-3727/42/21/214015
- Auradou H, Drazer G, Hulin JP, Koplik J (2005) Permeability anisotropy induced by the shear displacement of rough fracture walls. Water Resour Res 41(9):281. https://doi.org/10.1029/2005WR003938
- Becker MW, Shapiro AM (2003) Interpreting tracer breakthrough tailing from different forced-gradient tracer experiment configurations in fractured bedrock. Water Resour Res 39(1):3119. https://doi.org/ 10.1029/2001WR001190
- Berkowitz B (2002) Characterizing flow and transport in fractured geological media: a review. Adv Water Resour 25(8–12):861–884. https://doi.org/10.1016/S0309-1708(02)00042-8
- Bodvarsson GS (1972) Thermal problems in the siting of reinjection wells. Geothermics 1(2):63–66
- Bodvarsson GS, Tsang SC (1981) Injection and thermal breakthrough in fractured geothermal reservoirs. 87(B2), 83 pp
- Boschan A, Ippolito I, Chertcoff R, Auradou H, Talon L, Hulin JP (2008) Geometrical and Taylor dispersion in a fracture with random obstacles: an experimental study with fluids of different rheologies. Water Resour Res 44(6):67. https://doi.org/10.1029/2007WR006403
- Bouquain J, Meheust Y, Davy P (2011) Horizontal pre-asymptotic solute transport in a plane fracture with significant density contrasts. J Contam Hydrol 120–121:184–197. https://doi.org/10.1016/j. jconhyd.2010.08.002
- Boutt DF, Grasselli G, Fredrich JT, Cook BK, Williams JR (2006) Trapping zones: the effect of fracture roughness on the directional anisotropy of fluid flow and colloid transport in a single fracture.

- Geophys Res Lett 33(21):1365. https://doi.org/10.1029/2006GL027275
- Briggs S, Karney BW, Sleep BE (2017) Numerical modeling of the effects of roughness on flow and eddy formation in fractures. J Rock Mech Geotech Eng 9(1):105–115. https://doi.org/10.1016/j.jrmge. 2016.08.004
- Brown SR (1987) Fluid flow through rock joints: the effect of surface roughness. J Geophys Res 92. https://doi.org/10.1029/JB092iB02p01337
- Brush DJ, Thomson NR (2003) Fluid flow in synthetic rough-walled fractures: Navier-Stokes, Stokes, and local cubic law simulations. Water Resour Res 39(4):1337. https://doi.org/10.1029/ 2002WR001346
- Cardenas MB, Slottke DT, Ketcham RA, Sharp JM (2007) Navier-Stokes flow and transport simulations using real fractures shows heavy tailing due to eddies. Geophys Res Lett 34(14):1677. https://doi. org/10.1029/2007GL030545
- Chen T, Clauser C, Marquart G, Willbrand K, Büsing H (2016) Modeling anisotropic flow and heat transport by using mimetic finite differences. Adv Water Resour 94:441–456. https://doi.org/10.1016/j. advwatres.2016.06.006
- Chen Z, Qian J, Zhan H, Zhou Z, Wang J, Tan Y (2017) Effect of roughness on water flow through a synthetic single rough fracture. Environ Earth Sci 76(4):55. https://doi.org/10.1007/s12665-017-6470-7
- Coursenotes MIT (2009) Flow coursenotes 2.006: spring 2009. Massachusetts Institute of Technology, Boston, 704 pp
- Crandall D, Bromhal G, Karpyn ZT (2010) Numerical simulations examining the relationship between wall-roughness and fluid flow in rock fractures. Int J Rock Mech Min Sci 47(5):784–796. https://doi.org/10.1016/j.ijrmms.2010.03.015
- de Dreuzy J-R, Méheust Y, Pichot G (2012) Influence of fracture scale heterogeneity on the flow properties of three-dimensional discrete fracture networks (DFN). J Geophys Res Solid Earth 117(B11). https://doi.org/10.1029/2012JB009461
- Dijk PE, Berkowitz B (1999) Three-dimensional flow measurements in rock fractures. Water Resour Res 35(12):3955–3959. https://doi.org/ 10.1029/1999WR900200
- Fomin SA, Chugunov VA, Hashida T (2011) Non-Fickian mass transport in fractured porous media. Adv Water Resour 34(2):205–214. https://doi.org/10.1016/j.advwatres.2010.11.002
- Ge S (1997) A governing equation for fluid flow in rough fractures. Water Resour Res 33(1):53–61. https://doi.org/10.1029/96WR02588
- Grant AM, Clearwater J, Quinao J, Bixley PF, Le Brun M (eds) (2013)
 Thermal stimulation of geothermal wells: a review of field data.
 Proceedings World Geothermal Congress 2015, April 201,
 Melbourne, Australia, 7 pp
- Gringarten AC, Witherspoon PA, Ohnishi Y (1975) Theory of heat extraction from fractured hot dry rock. J Geophys Res 80(8):1120–1124. https://doi.org/10.1029/JB080i008p01120
- Guha Roy D, Singh TN (2016) Fluid flow through rough rock fractures: parametric study. Int J Geomech 16(3):4015067. https://doi.org/10.1061/(ASCE)GM.1943-5622.0000522
- Guo B, Fu P, Hao Y, Peters CA, Carrigan CR (2016) Thermal drawdown-induced flow channeling in a single fracture in EGS. Geothermics 61:46–62. https://doi.org/10.1016/j.geothermics.2016.01.004
- Ishibashi T, Watanabe N, Hirano N, Okamoto A, Tsuchiya N (2015) Beyond-laboratory-scale prediction for channeling flows through subsurface rock fractures with heterogeneous aperture distributions revealed by laboratory evaluation. J Geophys Res Solid Earth 120(1):106–124. https://doi.org/10.1002/2014JB011555
- Kang PK, Le Borgne T, Dentz M, Bour O, Juanes R (2015) Impact of velocity correlation and distribution on transport in fractured media: field evidence and theoretical model. Water Resour Res 51(2):940– 959. https://doi.org/10.1002/2014WR015799



Lavrov A (2013) Redirection and channelization of power-law fluid flow in a rough-walled fracture. Chem Eng Sci 99:81–88. https://doi.org/ 10.1016/j.ces.2013.05.045

- Le Goc R, de Dreuzy J-R, Davy P (2010) Statistical characteristics of flow as indicators of channeling in heterogeneous porous and fractured media. Adv Water Resour 33(3):257–269. https://doi.org/10. 1016/j.advwatres.2009.12.002
- Lee SH, Lee K-K, Yeo IW (2014) Assessment of the validity of Stokes and Reynolds equations for fluid flow through a rough-walled fracture with flow imaging. Geophys Res Lett 41(13):4578–4585. https://doi.org/10.1002/2014GL060481
- Li B, Jiang Y (2013) Quantitative estimation of fluid flow mechanism in rock fracture taking into account the influences of JRC and Reynolds number. J MMIJ 129(7):479–484. https://doi.org/10.2473/journalofmmij.129.479
- Luo S, Zhao Z, Peng H, Pu H (2016) The role of fracture surface roughness in macroscopic fluid flow and heat transfer in fractured rocks. Int J Rock Mech Min Sci 87:29–38. https://doi.org/10.1016/j.ijrmms.2016.05.006
- Méheust Y, Schmittbuhl J (2001) Geometrical heterogeneities and permeability anisotropy of rough fractures. J Geophys Res 106(B2): 2089–2102
- Méheust Y, Schmittbuhl J (2003) Scale effects related to flow in rough fractures. Pure Appl Geophys 160(5):1023–1050. https://doi.org/10. 1007/PL00012559
- Mourzenko VV, Thovert J-F, Adler PM (1995) Permeability of a single fracture: validity of the Reynolds equation. J Phys II 5(3):465–482. https://doi.org/10.1051/jp2:1995133
- Neuman SP (2005) Trends, prospects and challenges in quantifying flow and transport through fractured rocks. Hydrogeol J 13(1):124–147. https://doi.org/10.1007/s10040-004-0397-2
- Neuville A, Toussaint R, Schmittbuhl J (2011) Hydraulic transmissivity and heat exchange efficiency of rough fractures: a model based on low pass filtered apertures. Geophys J Int 186(3):1064–107
- Nicholl MJ, Detournay E (2001) Simulation of flow and transport in a single fracture: macroscopic effects of underestimating local head loss. Geophys Res Lett 22(23)
- Nicholl MJ, Rajaram H, Glass RJ, Detwiler R (1995) Saturated flow in a single fracture: evaluation of the Reynolds equation in measured aperture fields. Water Resour Res 35(11)
- Nigon B, Englert A, Pascal C, Saintot A (2017) Multi-scale characterization of joint surface roughness. J Geophys Res Solid Earth. https://doi.org/10.1002/2017JB014322
- Oron AP, Berkowitz B (1998) Flow in rock fractures: the local cubic law assumption reexamined. Water Resour Res 34:2811–2825
- Park C-K, Hahn P-S (1998) Effects of aperture density distribution on the flow through a rock fracture with line-source and line-collection. Journal of the Korean Nuclear Society 30(6):485–495
- Pollard DD, Aydin A (1988) Progress in understanding jointing over the past century. Geol Soc Am Bull 100(8):1181–1204. https://doi.org/10.1130/0016-7606(1988)100<1181:PIUJOT>2.3.CO;2
- Pruess K, Heel T, Shan C (eds) (2005) Tracer testing for estimating heat transfer area in fractured reservoirs. Proceedings World Geothermal Congress 2005, April 2005, Antalya, Turkey, 8 pp
- Renshaw CE (1995) On the relationship between mechanical and hydraulic apertures in rough-walled fractures. J Geophys Res 100(B12). https://doi.org/10.1029/95JB02159
- Schmittbuhl J, Steyer A, Jouniaux L, Toussaint R (2008) Fracture morphology and viscous transport. Int J Rock Mech Min Sci 45(3):422–430. https://doi.org/10.1016/j.ijrmms.2007.07.007

- Suzuki A, Fomin SA, Chugunov VA, Niibori Y, Hashida T (2016) Fractional diffusion modeling of heat transfer in porous and fractured media. Int J Heat Mass Transf 103:611–618. https://doi.org/10.1016/j.ijheatmasstransfer.2016.08.002
- Talon L, Auradou H, Hansen A (2010) Permeability of self-affine aperture fields. Phys Rev E Stat Nonlinear Soft Matter Phys 82(4 Pt 2): 46108. https://doi.org/10.1103/PhysRevE.82.046108
- Tang DH, Frind EO, Sudicky EA (1981) Contaminant transport in fractured porous media analytical solution for a single fracture. Water Resour Res 17(3). https://doi.org/10.1029/WR017i003p00555
- Vilarrasa V, Koyama T, Neretnieks I, Jing L (2011) Shear-induced flow channels in a single rock fracture and their effect on solute transport. Transp Porous Media 87(2):503–523. https://doi.org/10.1007/s11242-010-9698-1
- Watanabe N, Hirano N, Tsuchiya N (2008) Determination of aperture structure and fluid flow in a rock fracture by high-resolution numerical modeling on the basis of a flow-through experiment under confining pressure. Water Resour Res 44(6):649. https://doi.org/10.1029/2006WR005411
- Watanabe N, Ishibashi T, Hirano N, Ohsaki Y, Tsuchiya Y, Tamagawa T, Okabe H, Tsuchiya N (2013) Precise 3D numerical modeling of fracture flow coupled with X-ray computed tomography for reservoir core samples. SPE J 16(03):683–691. https://doi.org/10.2118/146643-PA
- Witherspoon PA, Wang JSY, Iwai K, Gale JE (1980) Validity of cubic law for fluid flow in a deformable rock fracture. Water Resour Res 16(6). https://doi.org/10.1029/WR016i006p01016
- Zhao C, Hobbs BE, Ord A, Peng S, Mühlhaus HB, Liu L (2004) Theoretical investigation of convective instability in inclined and fluid-saturated three-dimensional fault zones. Tectonophysics 387(1–4):47–64. https://doi.org/10.1016/j.tecto.2004.06.007
- Zhao C, Hobbs BE, Ord A, HORNBY P, Peng S, Liu L (2007) Mineral precipitation associated with vertical fault zones: the interaction of solute advection, diffusion and chemical kinetics. Geofluids 7(1):3– 18. https://doi.org/10.1111/j.1468-8123.2006.00156.x
- Zhao C, Hobbs BE, Hutter K, Ord A (eds) (2008) Convective and advective heat transfer in geological systems, advances in geophysical and environmental mechanics and mathematics. Springer, Heidelberg, Germany
- Zhao C, Hobbs BE, Ord A (2016) Chemical dissolution-front instability associated with water–rock reactions in groundwater hydrology: analyses of porosity-permeability relationship effects. J Hydrol 540:1078–1087. https://doi.org/10.1016/j.jhydrol.2016.07.022
- Zhao C, Hobbs B, Ord A (2017) A new alternative approach for investigating acidization dissolution front propagation in fluid-saturated carbonate rocks. Sci China Technol Sci 60(8):1197–1210. https://doi.org/10.1007/s11431-016-0666-1
- Zhao Z, Li B, Jiang Y (2014) Effects of fracture surface roughness on macroscopic fluid flow and solute transport in fracture networks. Rock Mech Rock Eng 47(6):2279–2286. https://doi.org/10.1007/ s00603-013-0497-1
- Zimmerman RW, Kumar S, Bodvarsson GS (1991) Lubrication theory analysis of the permeability of rough-walled fractures. Int J Rock Mech Min Sci Geomech Abstr 28(4):325–331. https://doi.org/10.1016/0148-9062(91)90597-F
- Zimmerman RW, Al-Yaarubi A, Pain CC, Grattoni CA (2004) Non-linear regimes of fluid flow in rock fractures. Int J Rock Mech Min Sci 41(3):384. https://doi.org/10.1016/j.ijrmms.2003.12.045
- Zou L, Jing L, Cvetkovic V (2017) Modeling of solute transport in a 3D rough-walled fracture–matrix system. Transp Porous Media 116(3): 1005–1029. https://doi.org/10.1007/s11242-016-0810-z

